

ples include the uniform magnetic field case, the Scarf potential (both hyperbolic and trigonometric), and the Morse potential along one spatial dimension [27].

Being more precise, supersymmetry in quantum mechanics is a theoretical framework that allows to map the solutions from a stationary Schrödinger problem in a static one-dimensional potential to another stationary Schrödinger problem with a different potential that is called the supersymmetric partner of the former. Supersymmetry is realized in different manners, such as the factorization method [28,29] and the Darboux transformation [30,31], which are equivalent. Here we adopt the formalism developed in [32,33] in which rather than starting from the solutions to a Riccati equation, new potentials are generated departing from the solutions of an initial wave equation.

We revisit the construction the propagator of 2D Dirac fermions in a background static magnetic field, which is relevant to monolayer graphene and related systems. For this purpose, we expand the propagator in the basis of Ritus functions, namely, the eigenfunctions of the operator $(\gamma \cdot \Pi)^2$ where Π is the canonical momentum operator that includes the effect of the external magnetic field through minimal coupling. We consider non-trivial magnetic background fields derived within a first order intertwining formalism [32,33] from the known solutions to the 2D Dirac equation in the case on a uniform and an exponentially decaying magnetic fields [16,25–27]. To achieve that goal and aiming a self-contained presentation of our findings, we have organized the remaining of the article as follows: In the next section we briefly present the Ritus method to derive the fermion propagator in an external magnetic field. In Sect. 3 we present the first order intertwining framework to generate further inhomogeneous magnetic field profiles from the supersymmetric cases obtained within first order supersymmetry. We then work out the explicit examples of non-trivial magnetic fields derived from the uniform and the exponentially decaying magnetic field in detail. In Sect. 4 we straightforwardly derive the charge and current densities from the constructed propagator. Finally, we conclude in Sect. 5.

2 Fermion propagator in external magnetic fields

We start our discussion of the construction of the fermion propagator in external magnetic fields within the Ritus formalism (see Ref. [26] for a pedagogical presentation of the framework). Such a construction is relevant for monolayer graphene and other 2D materials for which the charge carriers behave as Dirac fermions. Let us consider a magnetic field pointing perpendicularly to the plane of motion of Dirac fermions, in such a way that, working in a Landau-like gauge, we introduce an electromagnetic potential $A^\mu = (0, 0, W_0(x))$ ¹, where $W_0(x)$ is a scalar function such that $W_0'(x) = \partial_x W_0(x)$ defines the profile of the field. In these circumstances, the fermion propagator cannot be diagonalized on the basis of momentum eigenfunctions, because the asymptotic states of these fermions in a background magnetic fields do not correspond to plane waves. Motivated by this observation, we notice that the Green function for Dirac particles, $G(x, x')$, satisfies

$$((\gamma \cdot \Pi) - m)G(z, z') = \delta^{(3)}(z - z'), \quad (1)$$

with $z = (t, x, y)$, γ denoting the Dirac matrices (we consider the representation $\gamma^0 = \sigma_3$, $\gamma_1 = i\sigma_1$, and $\gamma^2 = i\sigma_2$ where σ_i are the Pauli matrices), $\Pi_\mu = i\partial_\mu + eA_\mu$ is the canonical momentum, and e is the elementary charge. Moreover, although for monolayer graphene the mass gap m vanishes, it becomes a relevant parameter in other systems, and that is why we keep it finite. Eventually, we discuss the limit $m \rightarrow 0$. Since $G(z, z')$ commutes with $(\gamma \cdot \Pi)^2$, we expand the propagator on the basis of the eigenfunctions of the later, namely, the functions $\mathbb{E}_p(z)$ satisfying

$$(\gamma \cdot \Pi)^2 \mathbb{E}_p(z) = p^2 \mathbb{E}_p(z), \quad (2)$$

where the eigenvalue p^2 can be any real number. We refer to the functions $\mathbb{E}_p(z)$ as the Ritus eigenfunctions [22–24]. It can be directly verified that these functions $\mathbb{E}_p(z)$ fulfill the closure and completeness relations

$$\int d^3z \bar{\mathbb{E}}_{p'}(z) \mathbb{E}_p(z) = \mathbb{I} \delta(p - p'), \quad (3a)$$

$$\int d^3p \mathbb{E}_p(z') \bar{\mathbb{E}}_p(z) = \mathbb{I} \delta(z - z'), \quad (3b)$$

with $\bar{\mathbb{E}}_p(z) = \gamma^0 \mathbb{E}_p^*(z) \gamma^0$ and \mathbb{I} is the 2×2 unit matrix.

In order to construct the Ritus eigenfunctions, we notice that the operator

$$(\gamma \cdot \Pi)^2 = \gamma^\mu \gamma^\nu \Pi_\mu \Pi_\nu = \Pi^2 + \frac{e}{2} \sigma^{\mu\nu} F_{\mu\nu}, \quad (4)$$

¹In our conventions, Greek indices $\mu, \nu, \dots = 0, 1, 2$, whereas Latin indices $i, j, \dots = 1, 2$.

where $F_{\mu\nu}$ is the field strength tensor and $\sigma^{\mu\nu} = i[\gamma^\mu, \gamma^\nu]/2$. For a static magnetic field pointing perpendicularly to the plane, the only non-vanishing components of these tensors are

$$F_{12} = -F_{21} = W_0'(x), \quad \sigma^{12} = \sigma_3. \quad (5)$$

Then, the eigenvalue Eq. (2) becomes

$$(\Pi^2 + e\sigma_3 W_0'(x))\mathbb{E}_p(z) = p^2\mathbb{E}_p(z), \quad (6)$$

from where we observe that the Ritus eigenfunctions are actually matrices, whose explicit form is

$$\mathbb{E}_p(z) = \begin{pmatrix} E_{p,+1}(z) & 0 \\ 0 & E_{p,-1}(z) \end{pmatrix}. \quad (7)$$

Notice that the subscript $p = (p_0, p_2, k)$ is a vector that denotes the eigenvalues of the operators $i\partial_t$, $-i\partial_y$, and \mathcal{H}_σ , respectively, and whose norm squared corresponds to the eigenvalue in Eq. (2). That is, the components of the vector p are the numbers such that

$$i\partial_t\mathbb{E}_p(z) = p_0\mathbb{E}_p(z), \quad -i\partial_y\mathbb{E}_p(z) = -p_2\mathbb{E}_p(z), \quad \mathcal{H}_\sigma\mathbb{E}_p(z) = k\mathbb{E}_p(z), \quad (8)$$

with $\mathcal{H}_\sigma = -(\gamma \cdot \Pi)^2 + \Pi_0^2$. These eigenvalues allow us to write the scalar functions as

$$E_{p,\sigma}(z) = e^{-i(p_0 t - p_2 y)} F_{k,p_2,\sigma}(x), \quad (9)$$

where $\sigma = \pm 1$ are the eigenvalues of σ_3 and the functions $F_{k,p_2,\sigma}(x)$ satisfy

$$[-\partial_x^2 + (p_2 + eW_0(x))^2 - e\sigma W_0'(x)]F_{k,p_2,\sigma} = kF_{k,p_2,\sigma}, \quad (10)$$

which corresponds to a Pauli equation for a particle with mass $m = 1/2$ and gyromagnetic factor $g = 2$. This equation possesses a supersymmetric structure as we will briefly discuss below. Thus, $F_{k,p_2,\sigma}(x)$ are the solutions of the equations in (10) associated to each of the supersymmetric-partner potentials

$$V_0^\sigma(x) = (p_2 + eW_0(x))^2 - e\sigma W_0'(x). \quad (11)$$

From now on, we fix the value $\sigma = 1$. Then, we have the required ingredients to construct the Ritus eigenfunctions from a first-order supersymmetric formalism.

3 Supersymmetric quantum mechanics

Similar to the case of the standard harmonic oscillator, the formalism of first-order supersymmetric quantum mechanics (1-SUSY QM) introduces two first-order differential operators L_0^\pm explicitly given by

$$L_0^\pm = \mp \frac{d}{dx} + W_0(x), \quad (12)$$

where $W_0(x)$ is known as the superpotential. Here, L_0^+ and L_0^- are adjoint operators to each other. With them, a pair of Hamiltonians \mathcal{H}_+ and \mathcal{H}_- , whose respectively spectra are k_n^+ and k_n^- , can be factorized as

$$\mathcal{H}_\pm = L_0^\pm L_0^\mp. \quad (13)$$

Here, the so-called intertwining operators L_0^\pm satisfy the relations

$$\mathcal{H}_\pm L_0^\pm = L_0^\pm \mathcal{H}_\mp. \quad (14)$$

By a simple inspection, one can recognize that in the construction presented in the above section, the functions $F_{k,p_2,\sigma}$ are related by a supersymmetric transformation. Indeed, the action of the intertwining operators L_0^\pm on the solutions of the Hamiltonians (10) is (see the left panel in Fig. 1)

$$F_{n,p_2,-1}(x) = \frac{L_0^- F_{n+1,p_2,+1}}{\sqrt{k_{n+1}^+}}, \quad F_{n+1,p_2,+1}(x) = \frac{L_0^+ F_{n,p_2,-1}}{\sqrt{k_n^-}}, \quad (15)$$

where the ground state, which is annihilated by the operator L_0^- , behaves as

$$F_{0,p_2,+1}(x) \sim \exp\left(-\int W_0(x)dx\right). \quad (16)$$

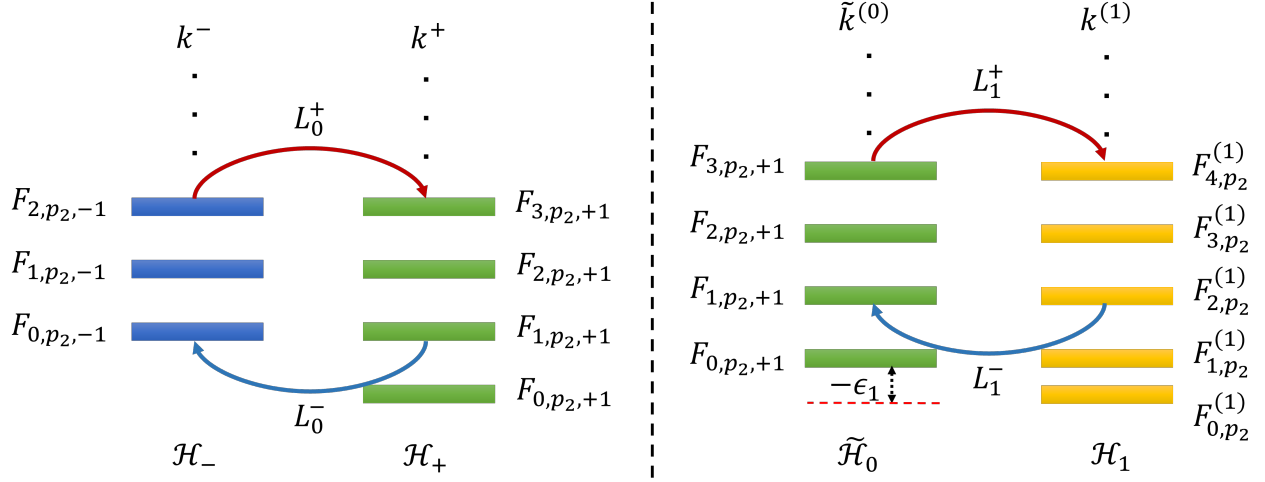


Figure 1: Representation of eigenfunctions $F_{k,p_2,\sigma}$ and $F_{k,p_2}^{(1)}$, and their corresponding energy levels for the chain of Hamiltonians. The intertwining relationship between the states in Eq. (9) is shown on the left, while the emergent relationship between the states $F_{k,p_2,+1}$ and the new functions $F_{k,p_2}^{(1)}$ is shown on the right.

This observation implies that we can write

$$W_0(x) = -\frac{F'_{0,p_2,+1}(x)}{F_{0,p_2,+1}(x)}. \quad (17)$$

Furthermore, the energy levels of \mathcal{H}_\pm turn out to be

$$k_n^- = k_{n+1}^+, \quad k_0^+ = 0. \quad (18)$$

These expressions indicate that the eigenfunctions and eigenvalues of the problem can be found through the operators L_0^\pm , which simplifies the calculations since this involves just first-order derivatives. Also, the magnetic field profile $B_0(x)$ can be related to the electromagnetic potential $A_\mu(x)$, the superpotential $W_0(x)$, and the ground state of H^+ as follows:

$$B_0(x) = A'_2(x) = \frac{1}{e} W'_0(x) = -\frac{1}{e} \frac{d^2}{dx^2} \{\ln[F_{0,p_2,+1}(x)]\}. \quad (19)$$

3.1 Generalized first order intertwining

In this section we introduce the first order supersymmetric formalism to generate inhomogeneous magnetic fields from intertwining operators. We follow closely the discussion of Ref. [33]. Taking as starting Hamiltonian the one with $\sigma = 1$ in (10), the first step of the method consists in displacing the energy of the Hamiltonian \mathcal{H}_+ as follows:

$$\tilde{\mathcal{H}}_0 \equiv \mathcal{H}_+ - \epsilon_1 = -\frac{d^2}{dx^2} + V_+(x) - \epsilon_1, \quad (20)$$

so that $\tilde{V}_0(x) = V_+(x) - \epsilon_1$, where $\epsilon_1 \leq k_0^+ = 0$. Here $\tilde{\mathcal{H}}_0$ is the Hamiltonian upon which the 1-SUSY QM formalism will be applied.

The second step is to build a new Hamiltonian \mathcal{H}_1 departing from $\tilde{\mathcal{H}}_0$ through the intertwining relation (see the right panel in Fig. 1):

$$\mathcal{H}_1 L_1^+ = L_1^+ \tilde{\mathcal{H}}_0, \quad (21)$$

where \mathcal{H}_1 and L_1^\pm are given by

$$\mathcal{H}_1 = -\frac{d^2}{dx^2} + V_1(x, \epsilon_1), \quad L_1^\pm = \mp \frac{d}{dx} + W_1(x, \epsilon_1), \quad (22)$$

respectively, which implies $\tilde{\mathcal{H}}_0 = L_1^- L_1^+$ and $\mathcal{H}_1 = L_1^+ L_1^-$. This leads to the following relations for W_1 and V_1 derived from V_0 ,

$$W_1^2(x, \epsilon_1) + W_1'(x, \epsilon_1) = \tilde{V}_0(x), \quad (23a)$$

$$V_1(x, \epsilon_1) = \tilde{V}_0(x) - 2W_1'(x, \epsilon_1). \quad (23b)$$

Let us suppose now that we can write $W_1(x, \epsilon_1) = u'_1/u_1$. The above relations lead us to the following expression for u_1 :

$$-u_1'' + \tilde{V}_0(x)u_1 = 0. \quad (24)$$

The corresponding magnetic field giving place to $V_1(x, \epsilon_1)$ is obtained from

$$B_1(x, \epsilon_1) = \frac{1}{e} \frac{dW_1(x, \epsilon_1)}{dx} = -B_0(x) - \frac{1}{e} \frac{d^2}{dx^2} \left\{ \ln \left[\frac{F_{0,p_2,+1}(x)}{u_1} \right] \right\}. \quad (25)$$

The third step of the method is to identify the eigenfunctions and eigenvalues of the new system. The energy levels for $\tilde{\mathcal{H}}_0$ and \mathcal{H}_1 are those of \mathcal{H}_+ , displaced by the quantity $-\epsilon_1$, plus the ground state of \mathcal{H}_1 at zero energy:

$$\tilde{k}_n^{(0)} = k_n^+ - \epsilon_1, \quad (26a)$$

$$k_0^{(1)} = 0, \quad k_{n+1}^{(1)} = \tilde{k}_n^{(0)}, \quad n = 0, 1, \dots, \quad (26b)$$

with $\epsilon_1 \leq k_0^+ = 0$. The unknown eigenfunctions associated with these energies are given by:

$$F_{0,p_2}^{(1)}(x) \sim \frac{1}{u_1}, \quad F_{n+1,p_2}^{(1)}(x) = \frac{1}{\sqrt{\tilde{k}_n^{(0)}}} L_1^+ F_{n,p_2,+1}(x). \quad (27)$$

where the eigenfunctions $F_{n,p_2,+1}(x)$ of \mathcal{H}_+ , and consequently those of $\tilde{\mathcal{H}}_0$, are assumed to be known. In addition, the ground state of \mathcal{H}_1 fulfills the condition $L_1^- F_{0,p_2}^{(1)}(x) = 0$.

It is worth noting that, according to the 1-SUSY QM formalism, since $\epsilon_1 \leq k_0^+$ and depending on the choice of the function u_1 , three different cases can arise for the spectrum of the Hamiltonian \mathcal{H}_1 : that it does not include the ground state of $\tilde{\mathcal{H}}_0$, or that it has an extra energy level, or that it is isospectral to $\tilde{\mathcal{H}}_0$. Below we discuss in detail two examples of magnetic field profiles, namely, the homogeneous field and the exponentially decaying magnetic field, only for one such case.

3.1.1 Uniform magnetic field

First, let us consider a uniform magnetic field, for which the vector potential is

$$\mathbf{A}(x) = B_0 x \hat{y} \implies \mathbf{B}_0(x) = B_0 \hat{z}, \quad (28)$$

and the corresponding superpotential reads as

$$W_0(x) = \frac{\omega}{2} x + p_2, \quad \omega = 2eB_0. \quad (29)$$

From this function, we obtain the superpartner potential which give explicitly that

$$\mathcal{H}_+ = -\frac{d^2}{dx^2} + V_+(x) = -\frac{d^2}{dx^2} + \frac{\omega^2}{4} \left(x + \frac{2p_2}{\omega} \right)^2 - \frac{\omega}{2}, \quad (30)$$

and its eigenenergies that correspond to those of a shifted quantum harmonic oscillator

$$k_n^+ = \omega n, \quad n = 0, 1, 2, \dots, \quad (31)$$

while the corresponding eigenfunctions can be expressed as

$$F_{n,p_2,+1}(x) = \sqrt{\frac{1}{2^n n!} \left(\frac{\omega}{2\pi} \right)^{1/2}} \exp \left(-\frac{\omega}{4} \left(x + \frac{2p_2}{\omega} \right)^2 \right) H_n \left[\sqrt{\frac{\omega}{2}} \left(x + \frac{2p_2}{\omega} \right) \right], \quad (32)$$

where $H_n(x)$ are the Hermite polynomials. By defining the dimensionless quantity

$$\eta(x) \equiv \sqrt{\frac{\omega}{2}} \left(x + \frac{2p_2}{\omega} \right), \quad (33)$$

we simplify the eigenfunctions as

$$F_{n,p_2,+1}(\eta) = \sqrt{\frac{1}{2^n n!} \left(\frac{\omega}{2\pi} \right)^{1/2}} \exp \left(-\frac{\eta^2}{2} \right) H_n(\eta). \quad (34)$$

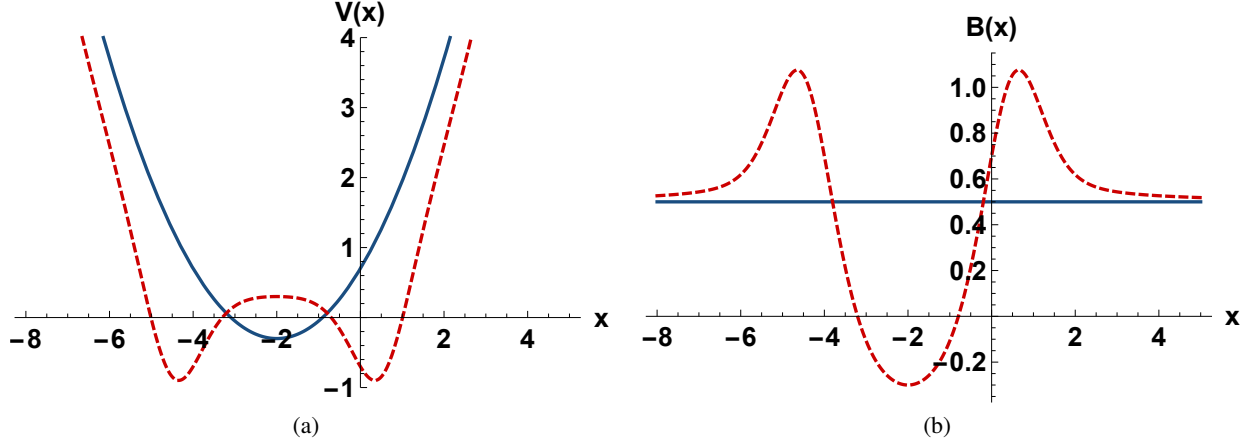


Figure 2: (a) Generated potential $V_1(x, \epsilon_1)$ (red, ---) and the initial one $\tilde{V}_0(x)$ (dark blue, —). (b) Generated magnetic field $B_1(x, \epsilon_1)$ (red, ---) and the constant initial one B_0 (dark blue, —). In both cases $B_0 = \frac{1}{2}$, $p_2 = 1$, $\epsilon_1 = -\frac{\omega}{5}$ and $\omega = 1$.

Next, we want to construct a different magnetic field profile starting from the uniform case by applying the 1-SUSY QM formalism. As stated earlier, the first step is to shift the energy of \mathcal{H}_+ as follows:

$$\tilde{\mathcal{H}}_0 = \mathcal{H}_+ - \epsilon_1 = -\frac{\omega}{2} \frac{d^2}{d\eta^2} + \frac{\omega}{2} \eta^2 - \frac{\omega}{2} - \epsilon_1, \quad (35)$$

with $\epsilon_1 \leq k_0^+ = 0$. Thus, the potential \tilde{V}_0 reads

$$\tilde{V}_0(\eta) = \frac{\omega}{2} \eta^2 - \frac{\omega}{2} - \epsilon_1. \quad (36)$$

From here, we can readily obtain $W_1(x, \epsilon_1)$ and correspondingly, $V_1(x, \epsilon_1)$. Then, from the replacement $W_1(x, \epsilon_1) = u_1'/u_1$ in Eq. (24), we easily infer that

$$u_1 = e^{-\eta^2/2} \left({}_1F_1 \left[a, \frac{1}{2}, \eta^2 \right] + 2\nu_1 \frac{\Gamma(a+1/2)}{\Gamma(a)} \eta {}_1F_1 \left[a + \frac{1}{2}, \frac{3}{2}, \eta^2 \right] \right), \quad (37)$$

with $a = -\epsilon_1/(2\omega)$, $\nu_1 \in (-1, 1)$. For definitiveness and comparison with the findings of Ref. [33], by choosing the parameters $\epsilon_1 = -k_1^+/5 = -\omega/5$ and $\nu_1 = 0$, we have $a = 1/10$ and

$$W_1(\eta, \epsilon_1) = \sqrt{\frac{\omega}{2}} \eta \left(-1 + \frac{2}{5} \frac{{}_1F_1 \left[\frac{11}{10}, \frac{3}{2}, \eta^2 \right]}{{}_1F_1 \left[\frac{1}{10}, \frac{1}{2}, \eta^2 \right]} \right), \quad (38a)$$

$$V_1(\eta, \epsilon_1) = \tilde{V}_0(\eta) - \sqrt{2\omega} \frac{d}{d\eta} \left[\sqrt{\frac{\omega}{2}} \eta \left(-1 + \frac{2}{5} \frac{{}_1F_1 \left[\frac{11}{10}, \frac{3}{2}, \eta^2 \right]}{{}_1F_1 \left[\frac{1}{10}, \frac{1}{2}, \eta^2 \right]} \right) \right], \quad (38b)$$

$$B_1(\eta, \epsilon_1) = -B_0 + \frac{2B_0}{5} \frac{d}{d\eta} \left[\sqrt{\frac{2}{\omega}} \eta \frac{{}_1F_1 \left[\frac{11}{10}, \frac{3}{2}, \eta^2 \right]}{{}_1F_1 \left[\frac{1}{10}, \frac{1}{2}, \eta^2 \right]} \right]. \quad (38c)$$

A plot of the generated potential $V_1(x, \epsilon_1)$ and the magnetic field profile $B_1(x, \epsilon_1)$ in this case is shown in Fig. 2. Then, the eigenenergies of the system are explicitly

$$k_0^{(1)} = 0, \quad k_{n+1}^{(1)} = \omega \left(n + \frac{1}{5} \right), \quad n = 0, 1, 2, \dots, \quad (39)$$

while the corresponding Ritus eigenfunctions, taking into account (9), are given by:

$$E_{0,p}^{(1)}(\eta, y, t) \sim \exp(-i(p_0 t - p_2 y)) \frac{\exp(\eta^2/2)}{{}_1F_1\left[\frac{1}{10}, \frac{1}{2}, \eta^2\right]}, \quad (40a)$$

$$\begin{aligned} E_{n+1,p}^{(1)}(x, y, t) &= \exp(-i(p_0 t - p_2 y)) F_{n+1,p_2}^{(1)}(x) \\ &= \exp(-i(p_0 t - p_2 y)) \frac{1}{\sqrt{\omega(n+1/5)}} L_1^+ F_{n,p_2,+1} \\ &= \frac{\exp(-i(p_0 t - p_2 y))}{\sqrt{2(n+1/5)}} \left(\frac{2\eta}{5} {}_1F_1\left[\frac{11}{10}, \frac{3}{2}, \eta^2\right] F_{n,p_2,+1} - \sqrt{2n} F_{n-1,p_2,+1} \right), \end{aligned} \quad (40b)$$

for $n = 0, 1, 2, \dots$. The joint choice of ϵ_1 and the function u_1 allows that the energy spectrum of \mathcal{H}_1 has an extra level in comparison with that of $\tilde{\mathcal{H}}_0$.

Inserting these expressions into Eq. (7), we obtain the Ritus eigenfunctions for a constant magnetic field for the graphene to first-order intertwining.

3.1.2 Exponentially decaying magnetic field

Let us now consider the vector potential

$$\mathbf{A}(x) = -\frac{B_0}{\alpha} (\exp(-\alpha x) - 1) \hat{y}, \quad B_0 > 1, \quad \alpha \geq 0, \quad (41)$$

where we refer to α as the inhomogeneity term.

Thus, we have

$$\mathbf{B}_0(x) = B_0 \exp(-\alpha x) \hat{z} \implies W_0(x) = p_2 - D(\exp(-\alpha x) - 1), \quad D = \frac{e B_0}{\alpha}, \quad (42)$$

which leads to the Morse potentials:

$$V_0^\sigma(x) = q_2^2 + D^2 \exp(-2\alpha x) - 2D \left(q_2 + \sigma \frac{\alpha}{2} \right) \exp(-\alpha x), \quad (43)$$

where $q_2 = p_2 + D$. Note that our results coincide with those in Refs. [33, 34] making the replacement $q_2 \rightarrow k_2$.

By defining the quantity

$$\rho(x) \equiv \frac{2D}{\alpha} \exp(-\alpha x), \quad (44)$$

the eigenfunctions $F_{n,p_2,+1}(\rho)$ of \mathcal{H}_+ are given by [33–35]

$$F_{n,p_2,+1}(\rho) = N_n \exp(-\rho/2) \rho^{(q_2/\alpha-n)} L_n^{2(q_2/\alpha-n)}(\rho), \quad n = 0, 1, 2, \dots \leq q_2/\alpha, \quad (45)$$

where N_n is the corresponding normalization constant and $L_n^\alpha(x)$ are the Laguerre polynomials, and its eigenenergies turn out to be

$$k_n^+ = \alpha n (2q_2 - \alpha n), \quad n = 0, 1, \dots \quad (46)$$

We chose $V_0^+(\rho)$ and displace it by $-\epsilon_1$ to produce $\tilde{V}_0(\rho)$, namely,

$$\tilde{V}_0(\rho) = q_2^2 + \frac{\alpha^2}{4} \rho^2 - \alpha \rho \left(q_2 + \frac{\alpha}{2} \right) - \epsilon_1. \quad (47)$$

Again, the new potential $V_1(\rho, \epsilon_1)$ depends on $W_1(\rho, \epsilon_1)$, which is a solution of the Riccati equation:

$$W_1^2(\rho, \epsilon_1) + W_1'(\rho, \epsilon_1) = \tilde{V}_0(\rho), \quad (48a)$$

$$V_1(\rho, \epsilon_1) = \tilde{V}_0(\rho) - 2W_1'(\rho, \epsilon_1). \quad (48b)$$

The new superpotential is written as $W_1(\rho, \epsilon_1) = u_1'/u_1$, with u_1 being the general solution of the Schrödinger equation

$$-u_1'' + \tilde{V}_0(\rho)u_1 = 0, \quad (49a)$$

$$u_1 = \exp(-\rho/2) \left(\frac{\alpha \rho}{2D} \right)^{\sqrt{q_2^2 - \epsilon_1}/\alpha} \left({}_1F_1[a, b, \rho] + \left(\frac{2q_2}{\alpha} \right) \left(1 + \frac{1}{\nu_1} \right) U[a, b, \rho] \right), \quad (49b)$$

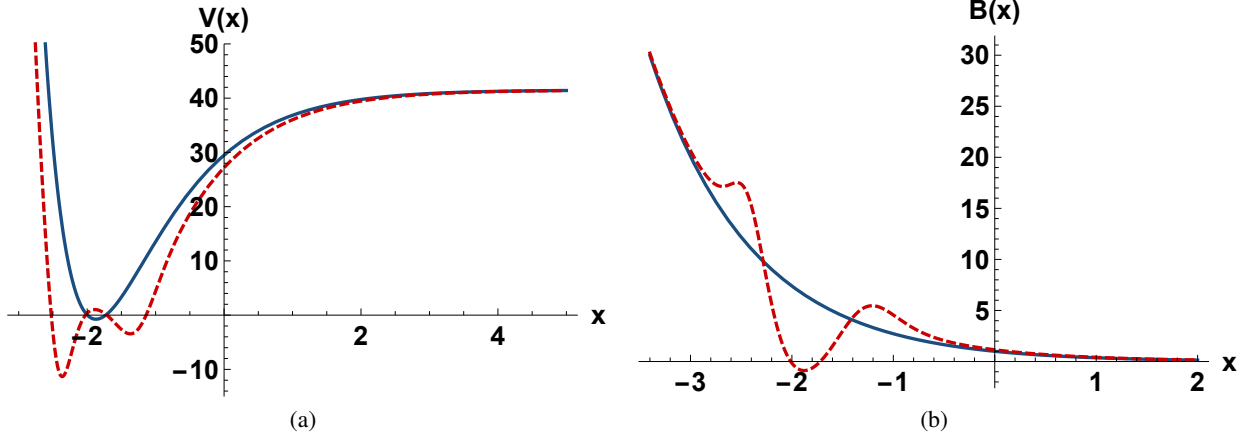


Figure 3: (a) Generated potential $V_1(x, \epsilon_1)$ (red, ---) and the initial one $\tilde{V}_0(x)$ (dark blue, —). (b) Generated magnetic field $B_1(x, \epsilon_1)$ (red, ---) and the initially decaying magnetic field (dark blue, —). In both cases $B_0 = 1$, $\nu_1 = -\frac{3}{2}$, $p_2 = 5\alpha$, $\epsilon_1 = -\frac{11\alpha^2}{2}$ and $\alpha = 1$.

where ν_1 obeys the restriction $\nu_1 \in \mathbb{R} - \{-1, 0\}$ and the parameters a and b are defined as:

$$a = -\frac{q_2}{\alpha} + \frac{\sqrt{q_2^2 - \epsilon_1}}{\alpha}, \quad b = 1 + \frac{2\sqrt{q_2^2 - \epsilon_1}}{\alpha}. \quad (50)$$

Therefore, the superpotential turns out to be:

$$W_1(\rho, \epsilon_1) = \frac{\alpha\rho}{2} - \sqrt{q_2^2 - \epsilon_1} + \mathcal{F}(\rho), \quad (51)$$

where the function $\mathcal{F}(\rho)$ reads

$$\mathcal{F}(\rho) = -\left(\frac{\alpha a}{b}\rho\right) \frac{{}_1F_1[1+a, 1+b, \rho] - \frac{2q_2b}{\alpha} \left(1 + \frac{1}{\nu_1}\right) U[1+a, 1+b, \rho]}{{}_1F_1[a, b, \rho] + \frac{2q_2}{\alpha} \left(1 + \frac{1}{\nu_1}\right) U[a, b, \rho]}. \quad (52)$$

Thus, the new potential and associated magnetic field are given by (see Eqs. (25) and (48b)):

$$V_1(\rho, \epsilon_1) = \tilde{V}_0(\rho) + 2\alpha\rho \frac{d}{d\rho} \left[\mathcal{F}(\rho) + \frac{\alpha\rho}{2} \right], \quad (53a)$$

$$B_1(\rho, \epsilon_1) = -\frac{\alpha^2\rho}{2e} - \frac{\alpha\rho}{e} \frac{d}{d\rho} \mathcal{F}(\rho). \quad (53b)$$

A plot of the generated potential $V_1(x, \epsilon_1)$ and the magnetic field profile $B_1(x, \epsilon_1)$ in this case is shown in Fig. 3.

In order to compare our results, we set the factorization energy as $\epsilon_1 = -k_1^+ / 2 = -\alpha(2q_2 - \alpha) / 2$, so the eigenenergies for the problem are given by:

$$k_0^{(1)} = 0, \quad k_{n+1}^{(1)} = \tilde{k}_n^{(0)} = \alpha n(2q_2 - \alpha n) + \frac{\alpha}{2}(2q_2 - \alpha), \quad n = 0, 1, \dots \quad (54)$$

The eigenfunctions corresponding to \mathcal{H}_1 take the form

$$F_{0,p_2}^{(1)}(\rho) \sim \frac{\exp(\rho/2) \left(\frac{2D}{\alpha\rho}\right)^{\sqrt{q_2^2 - \epsilon_1}/\alpha}}{{}_1F_1[a, b, \rho] + \left(\frac{2q_2}{\alpha}\right) \left(1 + \frac{1}{\nu_1}\right) U[a, b, \rho]}, \quad (55a)$$

$$\begin{aligned} F_{n+1,p_2}^{(1)}(\rho) &= \frac{1}{\sqrt{\alpha [n(2q_2 - \alpha n) + \frac{1}{2}(2q_2 - \alpha)]}} L_1^+(\rho, \epsilon_1) F_{n,p_2,+1}(\rho) \\ &= \frac{1}{\sqrt{\alpha [n(2q_2 - \alpha n) + \frac{1}{2}(2q_2 - \alpha)]}} \\ &\quad \times \left(\left(q_2 - \sqrt{q_2^2 - \epsilon_1} + \mathcal{F}(\rho) \right) - A^- \right) F_{n,p_2,+1}(\rho), \end{aligned} \quad (55b)$$

for $n = 0, 1, 2, \dots$, where

$$A^- = -\alpha\rho \frac{d}{d\rho} + \left(q_2 - \frac{\alpha\rho}{2}\right). \quad (56)$$

Therefore, the corresponding Ritus eigenfunctions, taking into account (9), are given by:

$$\begin{aligned} E_{0,p}^{(1)}(\rho, y, t) &= \exp(-i(p_0 t - p_2 y)) F_{0,p_2}^{(1)}(\rho) \\ &\sim \exp(-i(p_0 t - p_2 y)) \frac{\exp(\rho/2) \left(\frac{2D}{\alpha\rho}\right)^{\sqrt{q_2^2 - \epsilon_1}/\alpha}}{{}_1F_1[a, b, \rho] + \left(\frac{2q_2}{\alpha}\right) \left(1 + \frac{1}{\nu_1}\right) U[a, b, \rho]}, \end{aligned} \quad (57a)$$

$$\begin{aligned} E_{n+1,p}^{(1)}(x, y, t) &= \exp(-i(p_0 t - p_2 y)) F_{n+1,p_2}^{(1)}(x) \\ &= \exp(-i(p_0 t - p_2 y)) \frac{\left(\left(q_2 - \sqrt{q_2^2 - \epsilon_1} + \mathcal{F}(\rho)\right) - A^-\right) F_{n,p_2,+1}(\rho)}{\sqrt{\alpha} [n(2q_2 - \alpha n) + \frac{1}{2}(2q_2 - \alpha)]}, \end{aligned} \quad (57b)$$

for $n = 0, 1, 2, \dots$. Once again, the joint selection of ϵ_1 and u_1 allows that \mathcal{H}_1 has an extra energy level than $\tilde{\mathcal{H}}_0$.

Inserting these expressions into Eq. (7), we obtain the Ritus eigenfunctions for an exponentially decaying static magnetic field for the graphene to first-order intertwining.

4 Charge and current density

Physically, Ritus eigenfunctions $\mathbb{E}_p(z)$ correspond to the asymptotic states of graphene with momentum \bar{p} in the external field. Therefore, we can use these functions to diagonalize the fermion propagator $S(z, z')$ in momentum space in the same way plane waves are used to define the Fourier transform,

$$S(z, z') = \int d^3p \mathbb{E}_p(z) S(p) \bar{\mathbb{E}}_{p'}(z'). \quad (58)$$

Inserting this Green's functions in Eq. (1), using the property [36]

$$(\gamma \cdot \Pi) \mathbb{E}_p(z) = \mathbb{E}_p(z) (\gamma \cdot \bar{p}), \quad (59)$$

where the three-momentum vector $\bar{p} = (p_0, 0, \sqrt{k})$ satisfies $\bar{p}^2 = p^2 = p_0^2 - k$ [26] and the properties (3a), the propagator in momentum space takes the form

$$S_F(p) = \frac{1}{\gamma \cdot \bar{p} - m}, \quad (60)$$

similar to the free-particle propagator, but the momentum \bar{p} , which carries the quantum numbers induced on the dynamics of Dirac fermions by in the presence of the external field. In the configuration space, we write the propagator as

$$\begin{aligned} S(z, z') &= \int d^3p \mathbb{E}_p(z) \left[\frac{1}{\gamma \cdot \bar{p} - m} \right] \bar{\mathbb{E}}_{p'}(z') \\ &= \int d^3p \mathbb{E}_p(z) \left[\frac{\gamma \cdot \bar{p} + m}{p^2 - m^2} \right] \bar{\mathbb{E}}_{p'}(z'). \end{aligned} \quad (61)$$

From this expression we can find the value of the charge and induced vacuum current densities. First, we notice that we can write

$$\mathbb{E}_p = E_{p,+1} P_+ + E_{p,-1} P_-, \quad \bar{\mathbb{E}}_p = E_{p,+1}^* P_+ + E_{p,-1}^* P_-, \quad (62)$$

where we use projection operators $P_{\pm} = \frac{1}{2}(\mathbb{I} \pm \gamma^0) = \frac{1}{2}(\mathbb{I} \pm i\gamma^1\gamma^2)$, or more explicitly:

$$P_+ = \begin{pmatrix} 1 & 0 \\ 0 & 0 \end{pmatrix}, \quad P_- = \begin{pmatrix} 0 & 0 \\ 0 & 1 \end{pmatrix}, \quad (63)$$

which satisfy $P_{\pm} P_{\pm} = P_{\pm}$ and $P_{\pm} P_{\mp} = 0$. Hence, we have that

$$\begin{aligned} \text{Tr}\{\gamma^0 S(z, z')\} &= \text{Tr} \left\{ \gamma^0 \int d^3p \left[\frac{\gamma^\mu p_\mu + m}{p^2 - m^2} \right] (|E_{p,+1}|^2 P_+ + |E_{p,-1}|^2 P_-) \right\} \\ &= \int \frac{d^3p}{p^2 - m^2} \left(p_\mu \text{Tr} \left\{ \frac{\gamma^0 \gamma^\mu}{2} (|E_{p,+1}|^2 + |E_{p,-1}|^2) + \frac{\gamma^0 \gamma^\mu \gamma^0}{2} (|E_{p,+1}|^2 + |E_{p,-1}|^2) \right\} \right. \\ &\quad \left. + m \text{Tr} \left\{ \frac{\gamma^0}{2} (|E_{p,+1}|^2 + |E_{p,-1}|^2) + \frac{\gamma^0 \gamma^0}{2} (|E_{p,+1}|^2 + |E_{p,-1}|^2) \right\} \right). \end{aligned} \quad (64)$$

Upon taking traces, we obtain

$$\text{Tr}\{\gamma^0 S(z, z')\} = \int \frac{d^3 p}{p^2 - m^2} (p_0(|E_{p,+1}|^2 + |E_{p,-1}|^2) + m(|E_{p,+1}|^2 + |E_{p,-1}|^2)). \quad (65)$$

Therefore:

$$\begin{aligned} j^0 &= -ie \text{Tr}\{\gamma^0 S(z, z')\} \\ &= -ie \int \frac{d^3 p}{p^2 - m^2} \left(p_0(|E_{p,+1}|^2 + |E_{p,-1}|^2) + m(|E_{p,+1}|^2 + |E_{p,-1}|^2) \right). \end{aligned} \quad (66)$$

Since the first integral is odd respect to p_0 , we have that

$$j^0 = -ie \int \frac{d^3 p}{p^2 - m^2} m(|E_{p,+1}|^2 + |E_{p,-1}|^2). \quad (67)$$

On the other hand,

$$j^\ell = -ie \text{Tr}\{\gamma^\ell S(z, z')\}, \quad \ell = 1, 2, \quad (68)$$

where

$$\begin{aligned} \text{Tr}\{\gamma^\ell S(z, z')\} &= \int \frac{d^3 p}{p^2 - m^2} \left[\bar{p}_\mu \text{Tr}\{\gamma^\ell (E_{p,+1} P_+ + E_{p,-1} P_-) \gamma^\mu (E_{p,+1}^* P_+ + E_{p,-1}^* P_-)\} \right. \\ &\quad \left. + m \text{Tr}\{\gamma^\ell (E_{p,+1} P_+ + E_{p,-1} P_-) (E_{p,+1}^* P_+ + E_{p,-1}^* P_-)\} \right] \\ &= \int \frac{d^3 p}{p^2 - m^2} \left[\bar{p}_\mu \text{Tr} \left\{ \gamma^\ell \left[\frac{|E_{p,+1}|^2}{4} (\gamma^\mu + \gamma^\mu \gamma^0 + \gamma^0 \gamma^\mu + \gamma^0 \gamma^\mu \gamma^0) \right. \right. \right. \\ &\quad \left. \left. + \frac{E_{p,+1} E_{p,-1}^*}{4} (\gamma^\mu - \gamma^\mu \gamma^0 + \gamma^0 \gamma^\mu - \gamma^0 \gamma^\mu \gamma^0) \right. \right. \\ &\quad \left. \left. + \frac{E_{p,-1} E_{p,+1}^*}{4} (\gamma^\mu - \gamma^\mu \gamma^0 - \gamma^0 \gamma^\mu - \gamma^0 \gamma^\mu \gamma^0) \right. \right. \\ &\quad \left. \left. \frac{|E_{p,-1}|^2}{4} (\gamma^\mu + \gamma^\mu \gamma^0 - \gamma^0 \gamma^\mu + \gamma^0 \gamma^\mu \gamma^0) \right] \right\} \\ &\quad \left. + m \text{Tr} \left\{ \left(\frac{|E_{p,+1}|^2}{2} + \frac{|E_{p,-1}|^2}{2} \right) \gamma^\ell + \left(\frac{|E_{p,+1}|^2}{2} - \frac{|E_{p,-1}|^2}{2} \right) \gamma^\ell \gamma^0 \right\} \right]. \end{aligned} \quad (69)$$

Then, performing the traces with the aid of the identities

$$\text{Tr}\{\gamma^\ell \gamma^\mu\} = -2\delta^{\ell\mu}, \quad \text{Tr}\{\gamma^\ell \gamma^0 \gamma^\mu \gamma^0\} = \text{Tr}\{\gamma^\ell (2g^{\mu 0} - \gamma^\mu \gamma^0) \gamma^0\} = 2\delta^{\ell\mu}, \quad (70)$$

we have that

$$\begin{aligned} \text{Tr}\{\gamma^\ell S(z, z')\} &= \\ &= \int \frac{d^3 p}{p^2 - m^2} \bar{p}_\mu \left[\frac{|E_{p,+1}|^2}{4} (-2\delta^{\ell\mu} + 2\delta^{\ell\mu}) + \frac{E_{p,+1} E_{p,-1}^*}{4} (-2\delta^{\ell\mu} - 4i\varepsilon^{0\mu\ell} - 2\delta^{\ell\mu}) \right. \\ &\quad \left. + \frac{E_{p,-1} E_{p,+1}^*}{4} (-2\delta^{\ell\mu} - 4i\varepsilon^{0\mu\ell} - 2\delta^{\ell\mu}) + \frac{|E_{p,-1}|^2}{4} (-2\delta^{\ell\mu} + 2\delta^{\ell\mu}) \right]. \end{aligned} \quad (71)$$

Now, by taking $\bar{p} = (p_0, 0, \sqrt{k})$, it follows that

$$\text{Tr}\{\gamma^\ell S(z, z')\} = \int \frac{d^3 p}{p^2 - m^2} \alpha^{(\ell)} [E_{p,+1}^* E_{p,-1} + E_{p,+1} E_{p,-1}^*], \quad (72)$$

where $\alpha^{(\ell)} = i^\ell \sqrt{k}$ for $\ell = 1, 2$. Therefore,

$$j^\ell = -ie \int \frac{d^3 p}{p^2 - m^2} \alpha^{(\ell)} [E_{p,+1}^* E_{p,-1} + E_{p,+1} E_{p,-1}^*], \quad \ell = 1, 2. \quad (73)$$

In the next section we obtain the charge and current densities for the magnetic field profiles obtained in the previous section.

4.1 Charge and current density for a constant magnetic field

Inserting the explicit solutions of the Eqs. (40a) and (40b) into the Eq. (67), we obtain that the charge density to first order intertwining is

$$\begin{aligned}
 j^0 &= -ie \int dp_0 dp_2 \sum_{n=0}^{\infty} \frac{m}{p_0^2 - k_n^{(1)} - m^2} (|E_{p,+1}|^2 + |E_{p,-1}|^2) \\
 &= \pi e \int dp_2 \left[\text{sgn}(m) \rho_0(x, p_2) + \sum_{n=0}^{\infty} \frac{m}{\sqrt{m^2 + (n+1/5)\omega}} \rho_{n+1}(x, p_2) \right] \\
 &= \pi e \int dp_2 \left[\text{sgn}(m) |\mathcal{N}_0^{(1)}|^2 \frac{e^{\eta^2}}{({}_1F_1[\frac{1}{10}, \frac{1}{2}, \eta^2])^2} + \sum_{n=0}^{\infty} \frac{m}{\sqrt{m^2 + (n+1/5)\omega}} \right. \\
 &\quad \left. \times \left(\frac{|\mathcal{N}_{n+1}^{(1)}|^2}{2(n+1/5)} \left(\frac{2\eta}{5} {}_1F_1[\frac{11}{10}, \frac{3}{2}, \eta^2]} {}_1F_1[\frac{1}{10}, \frac{1}{2}, \eta^2]} F_{n,p_2,+1} - \sqrt{2n} F_{n-1,p_2,+1} \right)^2 + F_{n,p_2,+1}^2 \right) \right], \quad (74)
 \end{aligned}$$

where $\mathcal{N}_n^{(1)}$ denotes the corresponding normalization constants of the functions $E_{n,p}^{(1)}(x, y, t)$, and we have used the following result

$$\int_{-\infty}^{\infty} \frac{dp_0}{p_0^2 + b} = \frac{\pi}{\sqrt{b}}. \quad (75)$$

Similarly, inserting the explicit solutions of the Eqs. (40a) and (40b) into the Eq. (73), we obtain that the current density to first order intertwining is

$$\begin{aligned}
 j^\ell &= -ie \text{Tr}\{\gamma^\ell S(z, z')\} = -2i^{\ell+1} e \int dp_0 dp_2 \sum_{n=0}^{\infty} \frac{\sqrt{k_n^{(1)}}}{p_0^2 - k_n^{(1)} - m^2} E_{p,+1}^* E_{p,-1} \\
 &= -2i^\ell e \pi \int dp_2 \sum_{n=0}^{\infty} \frac{\sqrt{(n+1/5)\omega}}{\sqrt{m^2 + (n+1/5)\omega}} j_{n+1}(x, p_2) \\
 &= -2i^\ell e \pi \int dp_2 \sum_{n=0}^{\infty} \frac{\sqrt{(n+1/5)\omega}}{\sqrt{m^2 + (n+1/5)\omega}} \mathcal{N}_{n+1}^{(1)} \\
 &\quad \times \frac{F_{n,p_2,+1}}{\sqrt{2(n+1/5)}} \left(\frac{2\eta}{5} {}_1F_1[\frac{11}{10}, \frac{3}{2}, \eta^2]} {}_1F_1[\frac{1}{10}, \frac{1}{2}, \eta^2]} F_{n,p_2,+1} - \sqrt{2n} F_{n-1,p_2,+1} \right). \quad (76)
 \end{aligned}$$

With these expressions, it is customary to calculate the probability density and probability current. The probability density for the excited states of graphene is $\rho_{n+1}(x)$ and $\rho_0(x)$ for the ground state. The probability currents are $j_{n+1}(x)$ and $j_0(x) = 0$, respectively [34]. Some graphs for the probability density and probability current are shown in Figs. 4 and 5 that agree with [33].

4.2 Charge and current density for an exponentially decaying magnetic field

Inserting the explicit solutions of the Eqs. (57a) and (57b) into the Eq. (67), we obtain that the charge density to first order intertwining is

$$\begin{aligned}
 j^0 &= -ie \int dp_0 dp_2 \sum_{n=0}^{\infty} \frac{m}{p_0^2 - k_n^{(1)} - m^2} (|E_{p,+1}|^2 + |E_{p,-1}|^2) \\
 &= \pi e \int dp_2 \left[\text{sgn}(m) \rho_0(x, p_2) + \sum_{n=0}^{\infty} \frac{m}{\sqrt{m^2 + k_{n+1}^{(1)}}} \rho_{n+1}(x, p_2) \right] \\
 &= \pi e \int dp_2 \left[\text{sgn}(m) |\mathcal{N}_0^{(1)} F_{0,p_2}^{(1)}|^2 + \sum_{n=0}^{\infty} \frac{m}{\sqrt{m^2 + k_{n+1}^{(1)}}} \left(|\mathcal{N}_{n+1}^{(1)} F_{n+1,p_2}^{(1)}|^2 + |F_{n,p_2,+1}|^2 \right) \right]. \quad (77)
 \end{aligned}$$

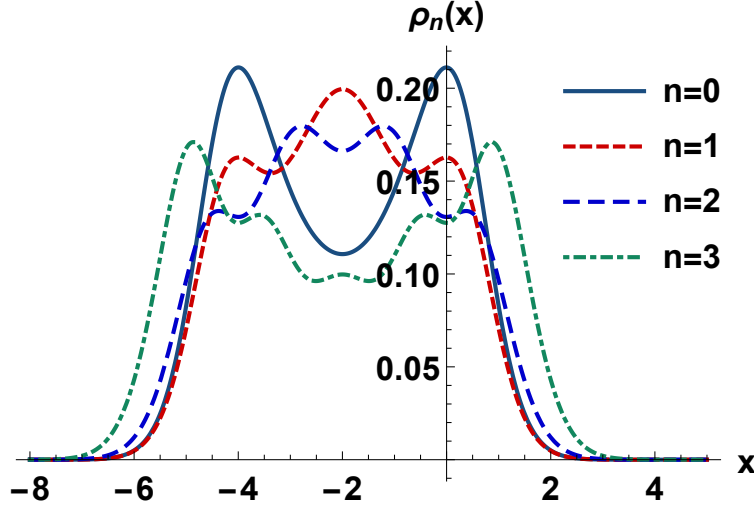


Figure 4: Probability density $\rho_0(x)$ for the ground state $n = 0$ (dark blue, —) and the excited states $\rho_{n+1}(x)$: $n = 0$ (red, ---), $n = 1$ (blue, -.-.-) and $n = 2$ (green, -.-.-). In all the cases $B_0 = \frac{1}{2}$, $p_2 = 1$, $\epsilon_1 = -\frac{\omega}{5}$ and $\omega = 1$.

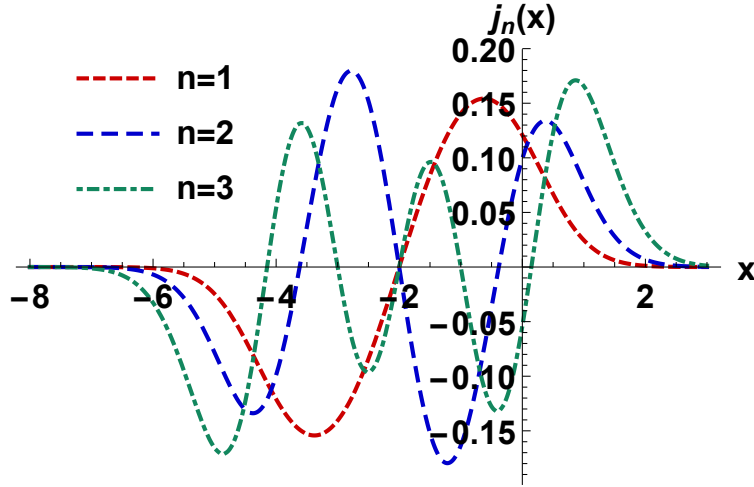


Figure 5: Current densities $j_{n+1}(x)$ for the excited states: $n = 0$ (red, ---), $n = 1$ (blue, -.-.-) and $n = 2$ (green, -.-.-). In all the cases $B_0 = \frac{1}{2}$, $p_2 = 1$, $\epsilon_1 = -\frac{\omega}{5}$ and $\omega = 1$.

Once again, inserting the explicit solutions of the Eqs. (57a) and (57b) into the Eq. (73), we obtain that the charge density to first order intertwining is

$$\begin{aligned}
 j^\ell &= -ie \operatorname{Tr}\{\gamma^\ell S(z, z')\} = -2i^{\ell+1}e \int dp_0 dp_2 \sum_{n=0}^{\infty} \frac{\sqrt{k_n^{(1)}}}{p_0^2 - k_n^{(1)} - m^2} E_{p,+1}^* E_{p,-1} \\
 &= -2i^\ell e \pi \int dp_2 \sum_{n=0}^{\infty} \frac{\sqrt{k_{n+1}^{(1)}}}{\sqrt{m^2 + k_{n+1}^{(1)}}} j_{n+1}(x, p_2) \\
 &= -2i^\ell e \pi \int dp_2 \sum_{n=0}^{\infty} \frac{\sqrt{k_{n+1}^{(1)}}}{\sqrt{m^2 + k_{n+1}^{(1)}}} \mathcal{N}_{n+1}^{(1)} F_{n,p_2,+1}(\rho) F_{n+1,p_2}^{(1)}(\rho). \tag{78}
 \end{aligned}$$

Thus, we calculate the probability density and probability current with these expressions, which are plotted in Figs. 6 and 7.

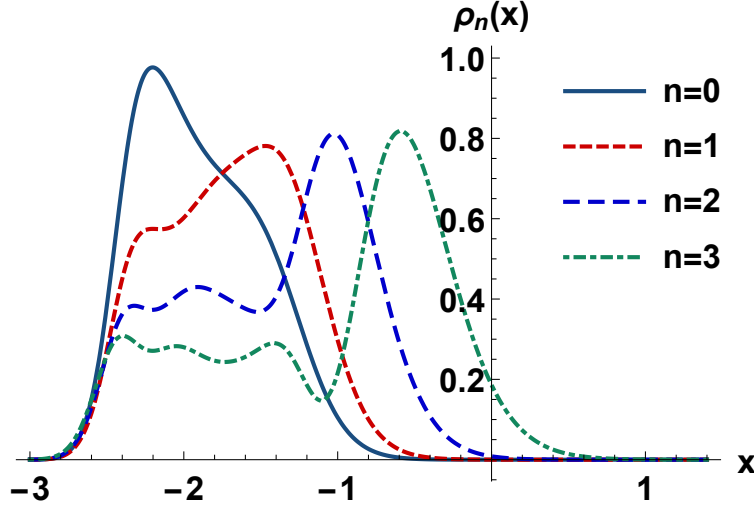


Figure 6: Probability density $\rho_0(x)$ for the ground state $n = 0$ (dark blue, —) and the excited states $\rho_{n+1}(x)$: $n = 0$ (red, ---), $n = 1$ (blue, ····) and $n = 2$ (green, -·-·). In all the cases $B_0 = 1$, $\nu_1 = -\frac{3}{2}$, $p_2 = 5\alpha$, $\epsilon_1 = -\frac{11\alpha^2}{2}$ and $\alpha = 1$.

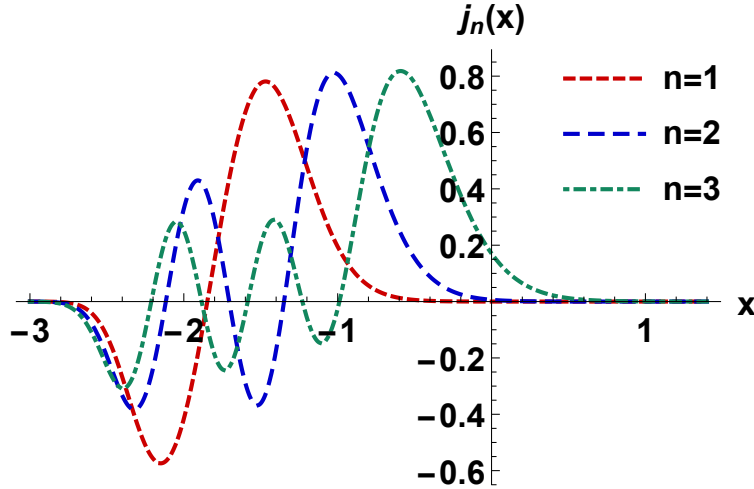


Figure 7: Current densities $j_{n+1}(x)$ for the excited states: $n = 0$ (red, ---), $n = 1$ (blue, ····) and $n = 2$ (green, -·-·). In all the cases $B_0 = 1$, $\nu_1 = -\frac{3}{2}$, $p_2 = 5\alpha$, $\epsilon_1 = -\frac{11\alpha^2}{2}$ and $\alpha = 1$.

4.3 Behavior for small inhomogeneity α

Let us consider the asymptotic behavior of the previous results for small values of the parameter α in order to compare them with those for the constant magnetic field case, since in the limit $\alpha \rightarrow 0$ the exponentially decaying magnetic field tends to the constant magnetic field.

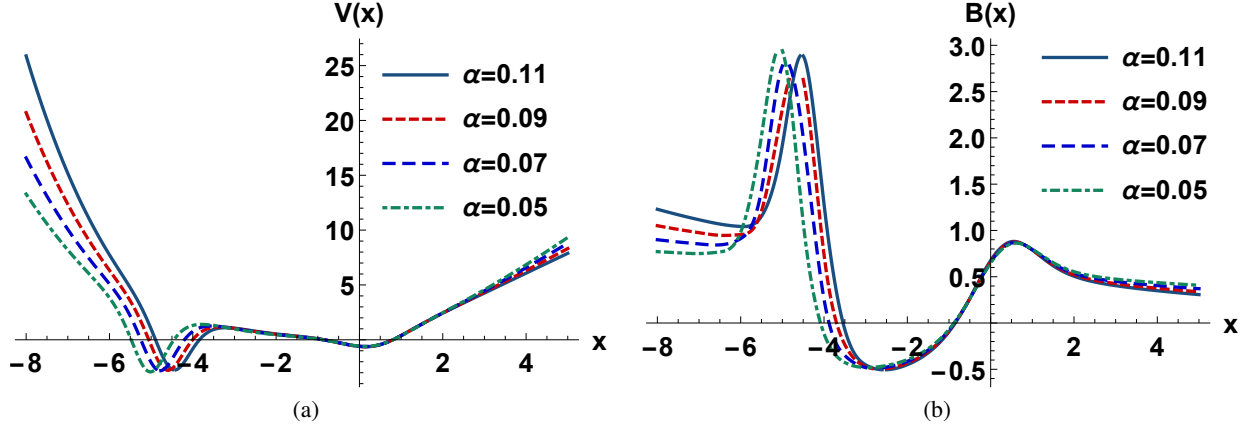


Figure 8: (a) Generated potential $V_1(x, \epsilon_1)$ in (53a) and (b) generated magnetic field $B_1(x, \epsilon_1)$ in (53b) for small inhomogeneity ($\alpha < 1$): $\alpha = 0.11$ (dark blue, —), $\alpha = 0.09$ (red, - - -), $\alpha = 0.07$ (blue, - · - ·) and $\alpha = 0.05$ (green, · · · ·). In all the cases $B_0 = \frac{1}{2}$, $\nu_1 = -\frac{3}{2}$, $p_2 = 1$ and $\epsilon_1 = -\frac{k_1^+}{5}$.

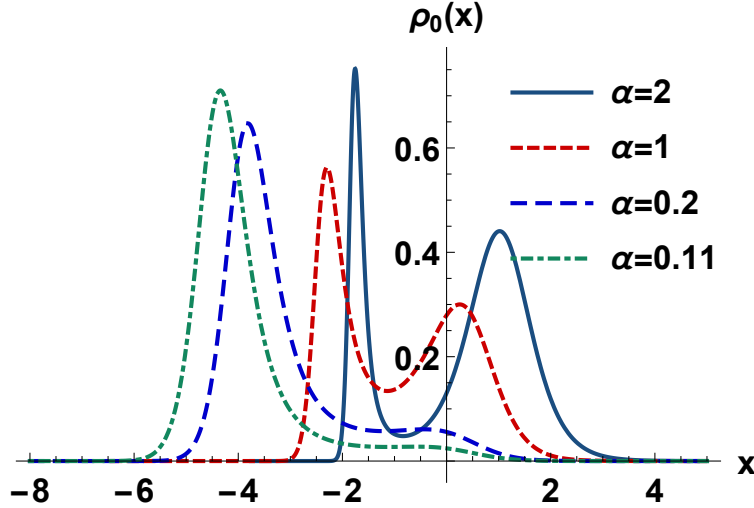


Figure 9: Probability density $\rho_0(x)$ for the ground state $n = 0$ in (57a) for different values of inhomogeneity: $\alpha = 2$ (dark blue, —), $\alpha = 1$ (red, - - -), $\alpha = 0.2$ (blue, - · - ·) and $\alpha = 0.11$ (green, · · · ·). In all the cases $B_0 = \frac{1}{2}$, $\nu_1 = -\frac{3}{2}$, $p_2 = 1$ and $\epsilon_1 = -\frac{k_1^+}{5}$.

Indeed, rewriting $D = \omega/(2\alpha)$, being ω as in Eq. (29), the superpotential $W_0(x)$, the Morse potential $V_0^-(x)$ and the eigenenergies k_n^+ in Eqs. (42), (43) and (46), respectively, turn into:

$$\lim_{\alpha \rightarrow 0} W_0(x) = \lim_{\alpha \rightarrow 0} p_2 - \frac{\omega}{2\alpha} (\exp(-\alpha x) - 1) = \frac{\omega}{2} x + p_2, \quad (79a)$$

$$\begin{aligned} \lim_{\alpha \rightarrow 0} V_0^-(x) &= \lim_{\alpha \rightarrow 0} \left(p_2 + \frac{\omega}{2\alpha} \right)^2 + \frac{\omega^2}{4\alpha^2} \exp(-2\alpha x) - \frac{\omega}{\alpha} \left(p_2 + \frac{\omega}{2\alpha} + \frac{\alpha}{2} \right) \exp(-\alpha x) \\ &= \frac{\omega^2}{4} \left(x + \frac{2p_2}{\omega} \right)^2 - \frac{\omega}{2}, \end{aligned} \quad (79b)$$

$$\lim_{\alpha \rightarrow 0} k_n^+ = \lim_{\alpha \rightarrow 0} \alpha n \left(2 \left[p_2 + \frac{\omega}{2\alpha} \right] - \alpha n \right) = \omega n, \quad n = 0, 1, \dots \quad (79c)$$

which coincide with Eqs. (29), (30) and (31), respectively. In Fig. 8, we show the behavior of the potential $V_1(x, \epsilon_1)$ and the magnetic field profile $B_1(x, \epsilon_1)$ for small values of α . According to the plots, for small inhomogeneity the potential and the magnetic field generated by the supersymmetric transformation have a similar behavior to their

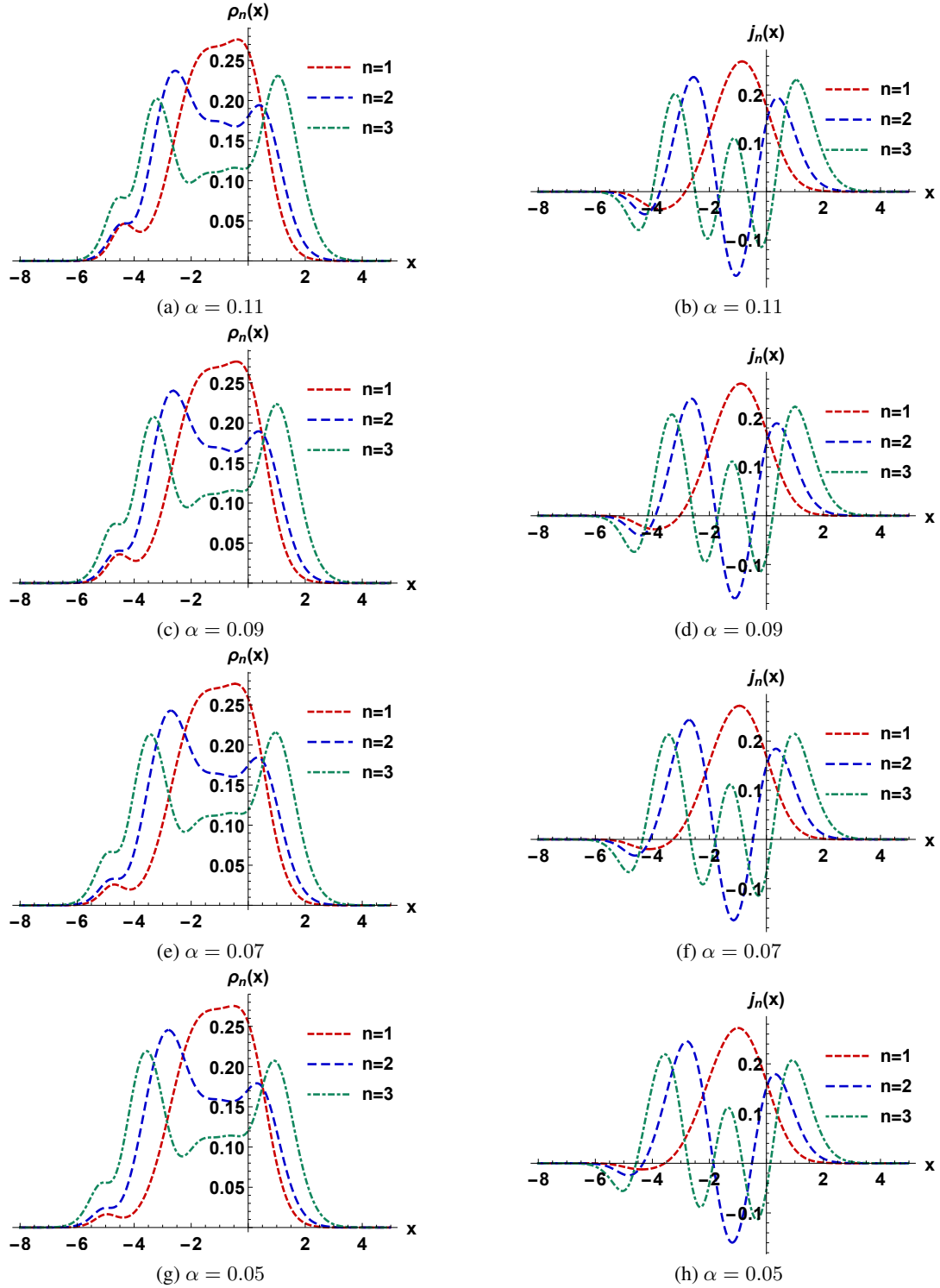


Figure 10: Probability density $\rho_0(x)$ (left-hand) and current densities $j_{n+1}(x)$ (right-hand) for the excited states in (57b): $n = 0$ (red, ---), $n = 1$ (blue, -·-·-) and $n = 2$ (green, -·-·-). In all the cases $B_0 = \frac{1}{2}$, $\nu_1 = -\frac{3}{2}$, $p_2 = 1$, $\epsilon_1 = -\frac{k_1^+}{5}$ and small inhomogeneity ($\alpha < 1$).

counterparts in the constant magnetic field case for $|x| \rightarrow \infty$, while for values of x in the inner region of $V_1(x, \epsilon_1)$ and $B_1(x, \epsilon_1)$, such functions do not look like those in Fig. 2.

On the other hand, the probability density $\rho_0(x)$ does not look like the corresponding one for the constant magnetic field case, as shown in Fig. 9. This suggests us that after the supersymmetric transformation is implemented to the exponentially decaying magnetic field case, we are not able to recover the eigenfunction $F_{0,p_2}^{(1)} \sim 1/u_1$ for the ground state of the Hamiltonian \mathcal{H}_1 of the constant magnetic field case. Likewise, the corresponding probability density and probability current for small values of α and $\epsilon_1 = -k_1^+/5$ are shown in Fig. 10. As we can see, the probability densities $\rho_n(x)$ and the current densities $j_n(x)$ for the excited states with $n > 1$ exhibit a subtle resemblance to the plots shown in Figs. 4 and 5 for a constant magnetic field $B_0 = 1/2$ and $p_2 = 1$. However, such functions are asymmetric respect to $x = -2$ in comparison with those that correspond to the eigenfunctions in Eqs. (40a) and (40b).

5 Final remarks

In this work, we have studied the Dirac fermion propagator for graphene-like systems in external magnetic fields. We have constructed the Dirac fermion propagator for graphene-like systems in the presence of non-trivial and inhomogeneous external magnetic fields generated by first-order intertwining operators from the solutions to the Dirac equation for a constant magnetic field and an exponentially decaying magnetic field [27, 34, 37–40]. We constructed the propagator in the basis of the eigenfunctions of the operator $(\gamma \cdot \Pi)^2$.

The generalized first-order intertwining method presented here have been followed of the discussion in Ref. [32, 33]. By choosing the parameters $\epsilon_1 = -k_1^+/5 = -\omega/5$ and $\nu_1 = 0$, we have obtained the generated potential $V_1(x, \epsilon_1)$ and the magnetic field profile $B_1(x, \epsilon_1)$ for the case of the uniform magnetic field whose graphs have been plotted in Fig. 2 and that agree with [33]. Similarly, taking $\epsilon_1 = -k_1^+/2 = -\alpha(2q_2 - \alpha)/2$ and the restriction $\nu_1 \in \mathbb{R} - \{-1, 0\}$, we obtained the generated potential $V_1(x, \epsilon_1)$ and the magnetic field profile $B_1(x, \epsilon_1)$ for the case of the exponentially decaying magnetic field whose graphs have been plotted in Fig. 3 and that agree with [33] too. In both cases, the energy spectrum of the corresponding Hamiltonian \mathcal{H}_1 has one more level than $\tilde{\mathcal{H}}_0$ derived from the selection of the parameter ϵ_1 and the function u_1 .

On the other hand, we have found the charge and current densities for the examples of inhomogeneous fields derived from the intertwining framework. From such densities, the probability density and the probability current for both cases of fields have been obtained and plotted in Figs. 4, 5, 6 and 7 for the ground state $n = 0$ and some excited states that reproduce the densities in the literature [33].

Additionally, we have shown that for the limit $\alpha \rightarrow 0$ the exponentially decaying magnetic field tends to the constant magnetic field. Thus, taking the limit $\alpha \rightarrow 0$ in the exponentially decaying magnetic field Morse potentials (Eqs. (42), (43)) and eigenenergies (Eq. (46)), respectively, we have obtained the Morse potential $V_0^+(x)$ (Eqs. (79b), (79a)) and the eigenenergies k_n^+ (Eq. (79c)) that coincide with the superpotential (Eqs. (29), (30)) and eigenenergies (Eq. (31)) of the uniform magnetic field case, respectively. Also, we have shown that for small inhomogeneity α the behavior of the potential $V_1(x, \epsilon_1)$ and the magnetic field profile $B_1(x, \epsilon_1)$ in general does not coincide with the uniform magnetic field case, except in the asymptotic limit $|x| \rightarrow \infty$.

Moreover, we have plotted the probability density taking the limit $\alpha \rightarrow 0$ in order to recover the probability density of the uniform magnetic field case, however this does not occur with our results as the Fig. 9 shown because after the supersymmetric transformation is implemented to the exponentially decaying magnetic field case, we have not recovered the eigenfunction $F_{0,p_2}^{(1)} \sim 1/u_1$ for the ground state of the Hamiltonian \mathcal{H}_1 of the constant magnetic field case. For small values of α and $\epsilon_1 = -k_1^+/5$ we have obtained the probability density and probability current as shown in Fig. 10 where the plots are not symmetric respect to $x = -2$, as occurs in Figs. 4 and 5 for the excited states.

We think to obtain in the future the Ritus functions for graphene-like systems for the fields studied in this work by second-order intertwining operators. Results will be reported elsewhere. This work is hoped that will became a guide for colleagues interested in the theoretical developments of graphene-like systems.

Acknowledgments

EDB and AR acknowledge financial support from CONACYT Project FORDECYT-PRONACES/61533/2020. EDB also acknowledges the SIP-IPN research grant 20210317. YCS acknowledges the CIC-UMSNH research grant 6297771/2021.

References

- [1] V. A. Miransky and I. A. Shovkovy, “Quantum field theory in a magnetic field: From quantum chromodynamics to graphene and Dirac semimetals,” *Physics Reports*, vol. 576, pp. 1–209, 2015. Quantum field theory in a magnetic field: From quantum chromodynamics to graphene and Dirac semimetals.
- [2] P. R. Wallace, “The band theory of graphite,” *Phys. Rev.*, vol. 71, pp. 622–634, May 1947.
- [3] E. C. Marino, *Quantum Field Theory Approach to Condensed Matter Physics*. Cambridge University Press, 2017.
- [4] S. Shen, *Topological Insulators: Dirac Equation in Condensed Matter*. Springer Series in Solid-State Sciences, Springer Singapore, 2017.
- [5] Y. Zhang, Y.-W. Tan, H. L. Stormer, and P. Kim, “Experimental observation of the quantum hall effect and berry’s phase in graphene,” *Nature*, vol. 438, pp. 201–204, 2005.
- [6] J. R. Williams, L. DiCarlo, and C. M. Marcus, “Quantum Hall effect in a gate-controlled p-n junction in graphene,” *Science*, vol. 317, pp. 638–41, 2007.
- [7] K. S. Novoselov, Z. Jiang, Y. Zhang, S. V. Morozov, H. L. Stormer, U. Zeitler, J. C. Maan, G. S. Boebinger, P. Kim, and A. K. Geim, “Room-Temperature Quantum Hall Effect in Graphene,” *Science*, vol. 315, pp. 1379–1379, 2007.
- [8] M. Oliva-Leyva and C. Wang, “Magneto-optical conductivity of anisotropic two-dimensional Dirac-Weyl materials,” *Ann. Phys., NY*, vol. 384, pp. 61–70, 2017.
- [9] K. S. Novoselov, A. K. Geim, S. V. Morozov, D. Jiang, Y. Zhang, S. V. Dubonos, I. V. Grigorieva, and A. A. Firsov, “Electric field effect in atomically thin carbon films,” *Science*, vol. 306, p. 666, 2004.
- [10] G. G. Naumis, S. Barraza-Lopez, M. Oliva-Leyva, and H. Terrones, “Electronic and optical properties of strained graphene and other strained “d materials: a review,” *Rep. Prog. Phys.*, vol. 80, p. 096501, 2017.
- [11] K. S. Novoselov, A. K. Geim, S. V. Morozov, D. Jiang, M. I. Katsnelson, I. V. Grigorieva, S. V. Dubonos, and A. A. Firsov, “Two-dimensional gas of massless Dirac fermions in graphene,” *Nature*, vol. 438, pp. 197–200, 2005.
- [12] S. Das, J. A. Robinson, M. Dubey, H. Terrones, and M. Terrones, “Beyond Graphene: Progress in Novel Two-Dimensional Materials and van der Waals Solids,” *Annual Review of Materials Research*, vol. 45, no. 1, pp. 1–27, 2015.
- [13] D. Akinwande, C. J. Brennan, J. S. Bunch, P. Egberts, J. R. Felts, H. Gao, R. Huang, J.-S. Kim, T. Li, Y. Li, K. M. Liechti, N. Lu, H. S. Park, E. J. Reed, P. Wang, B. I. Yakobson, T. Zhang, Y.-W. Zhang, Y. Zhou, and Y. Zhu, “A review on mechanics and mechanical properties of 2D materials—Graphene and beyond,” *Extreme Mechanics Letters*, vol. 13, pp. 42–77, 2017.
- [14] P. Bazylewski and G. Fanchini, “1.13 - graphene: Properties and applications,” in *Comprehensive Nanoscience and Nanotechnology (Second Edition)* (D. L. Andrews, R. H. Lipson, and T. Nann, eds.), pp. 287–304, Oxford: Academic Press, second edition ed., 2019.
- [15] C. Chang, W. Chen, Y. Chen, Y. Chen, Y. Chen, F. Ding, C. Fan, H. J. Fan, Z. Fan, C. Gong, Y. Gong, Q. He, X. Hong, S. Hu, W. Hu, W. Huang, Y. Huang, W. Ji, D. Li, L.-J. Li, Q. Li, L. Lin, C. Ling, M. Liu, N. Liu, Z. Liu, K. P. Loh, J. Ma, F. Miao, H. Peng, M. Shao, L. Song, S. Su, S. Sun, C. Tan, Z. Tang, D. Wang, H. Wang, J. Wang, X. Wang, X. Wang, A. T. S. Wee, Z. Wei, Y. Wu, Z.-S. Wu, J. Xiong, Q. Xiong, W. Xu, P. Yin, H. Zeng, Z. Zeng, T. Zhai, H. Zhang, H. Zhang, Q. Zhang, T. Zhang, X. Zhang, L.-D. Zhao, M. Zhao, W. Zhao, Y. Zhao, K.-G. Zhou, X. Zhou, Y. Zhou, H. Zhu, H. Zhang, and Z. Liu, “Recent progress on two-dimensional materials,” *Acta Physico-Chimica Sinica*, vol. 37, no. 12, p. 2108017, 2021.
- [16] P. Roy, T. K. Ghosh, and K. Bhattacharya, “Localization of Dirac-like excitations in graphene in the presence of smooth inhomogeneous magnetic fields,” *Journal of Physics: Condensed Matter*, vol. 24, p. 055301, jan 2012.
- [17] M. Vozmediano, M. Katsnelson, and F. Guinea, “Gauge fields in graphene,” *Physics Reports*, vol. 496, no. 4, pp. 109–148, 2010.
- [18] J. Lin and W. Zhou, “6 - Defect in 2D materials beyond graphene,” in *Defects in Advanced Electronic Materials and Novel Low Dimensional Structures* (J. Stehr, I. Buyanova, and W. Chen, eds.), Woodhead Publishing Series in Electronic and Optical Materials, pp. 161–187, Woodhead Publishing, 2018.
- [19] G. G. Naumis, “Electronic properties of 2D materials and its heterostructures: a minimal review,” *Revista Mexicana de Física*, vol. 67, no. 5, p. 050102, 2021.

- [20] J. Schwinger, “On gauge invariance and vacuum polarization,” *Phys. Rev.*, vol. 82, pp. 664–679, Jun 1951.
- [21] J. Suzuki, “Quantum electrodynamics in a uniform magnetic field.” hep-th/0512329.
- [22] V. Ritus, “Radiative corrections in quantum electrodynamics with intense field and their analytical properties,” *Annals of Physics*, vol. 69, no. 2, pp. 555–582, 1972.
- [23] V. I. Ritus, “Diagonality of electron mass operator in a constant field,” *Pisma Zh. Eksp. Teor. Fiz.*, vol. 20, pp. 135–138, 1974.
- [24] V. I. Ritus, “Eigenfunction method and mass operator in the quantum electrodynamics of a constant field,” *Pisma Zh. Eksp. Teor. Fiz.*, vol. 75, pp. 1560–1583, 1978.
- [25] A. Raya and E. Reyes, “Fermion condensate and vacuum current density induced by homogeneous and inhomogeneous magnetic fields in $(2 + 1)$ dimensions,” *Phys. Rev. D*, vol. 82, p. 016004, Jul 2010.
- [26] G. Murguía, A. Raya, A. Sánchez, and E. Reyes, “The electron propagator in external electromagnetic fields in low dimensions,” *American Journal of Physics*, vol. 78, no. 7, pp. 700–707, 2010.
- [27] Y. Concha, A. Huet, A. Raya, and D. Valenzuela, “Supersymmetric quantum electronic states in graphene under uniaxial strain,” *Mater. Res. Express*, vol. 5, p. 065607, jun 2018.
- [28] B. Mielnik, “Factorization method and new potentials with the oscillator spectrum,” *Journal of Mathematical Physics*, vol. 25, no. 12, pp. 3387–3389, 1984.
- [29] M. S. Berger and N. S. Ussembayev, “Isospectral potentials from modified factorization,” *Phys. Rev. A*, vol. 82, p. 022121, Aug 2010.
- [30] G. Darboux, “On a proposition relative to linear equations,” *CR Acad. Sci. Paris*, vol. 94, no. physics/9908003, pp. 1456–59, 1882.
- [31] V. B. Matveev and V. Matveev, *Darboux transformations and solitons*. Springer-Verlag, 1991.
- [32] B. Midya and D. J. Fernández, “Dirac electron in graphene under supersymmetry generated magnetic fields,” *Journal of Physics A: Mathematical and Theoretical*, vol. 47, p. 285302, jun 2014.
- [33] M. Castillo-Celeita and D. J. Fernández C, “Dirac electron in graphene with magnetic fields arising from first-order intertwining operators,” *Journal of Physics A: Mathematical and Theoretical*, vol. 53, p. 035302, jan 2020.
- [34] Ş. Kuru, J. Negro, and L. M. Nieto, “Exact analytic solutions for a Dirac electron moving in graphene under magnetic fields,” *Journal of Physics: Condensed Matter*, vol. 21, p. 455305, oct 2009.
- [35] T. K. Ghosh, “Exact solutions for a Dirac electron in an exponentially decaying magnetic field,” *Journal of Physics: Condensed Matter*, vol. 21, p. 045505, dec 2008.
- [36] F. Cooper, A. Khare, and U. Sukhatme, “Supersymmetry and quantum mechanics,” *Phys. Rep.*, vol. 251, pp. 267–385, jan 1995.
- [37] E. Milpas, M. Torres, and G. Murguía, “Magnetic field barriers in graphene: an analytically solvable model,” *Journal of Physics: Condensed Matter*, vol. 23, p. 245304, jun 2011.
- [38] V. Jakubský and D. Krejčířík, “Qualitative analysis of trapped Dirac fermions in graphene,” *Ann. Phys., NY*, vol. 349, pp. 268–287, oct 2014.
- [39] V. Jakubský, “Spectrally isomorphic Dirac systems: graphene in a electromagnetic field,” *Phys. Rev D*, vol. 91, p. 045039, feb 2015.
- [40] D. Jahani, F. Shahbazi, and M. R. Setare, “Magnetic dispersion of Dirac fermions in graphene under inhomogeneous field profiles,” *Eur. Phys. J. Plus*, vol. 133, p. 328, aug 2018.